17èmes JOURNEES DE L'HYDRODYNAMIQUE
JH2020

24 - 26 novembre 2020
CHERBOURG - en - COTENTIN

Experimental investigation of the seabed roughness effect on the hydrodynamical behavior of a submarine cable under current and wave conditions.

A. Marty[(1),*], G. Damblans[(2)], J-V. Facq[(1)], B. Gaurier[(1)], G. Germain[(1)], N. Germain[(2)], J. Harris[(4)], A. Maison[(2)], C. Peyrard[(3)], and N. Relun[(3)]

[(1)]IFREMER, Marine Structure Laboratory, 150 Quai Gambetta, Boulogne/Mer, France
[(2)]France Energies Marines, Brest, France
[(3)]EDF R&D, 6 Quai Watier, 78400 Chatou, France
[(4)]LHSV, Ecole des Ponts, CEREMA, EDF R&D, Chatou, France
[*]Corresponding author: antoine.marty@ifremer.fr

Résumé

Le comportement des câbles sous-marins est étudié expérimentalement dans le cadre du projet France Energies Marines STHYF. Dans le but d'évaluer la stabilité des câbles lorsqu'ils sont placés sur des fonds avec de grandes rugosités et soumis à de fortes conditions de vagues et de courants, les efforts hydrodynamiques qui se produisent sur un cylindre fixe placé à proximité d'une plaque sur laquelle est positionné ou non des éléments de rugosités ont été mesurés. Des sollicitations spécifiques (courant, oscillations forcées et oscillations + courant) sont imposées afin de quantifier les efforts hydrodynamiques exercés sur le cylindre placé à différents distances de la plaque (avec ou sans rugosité). Les effets de la rugosité sur les efforts appliqués au cylindre et sur l'écoulement sont étudiés et mettent en évidence des différences importantes entre la configuration fond rugueux et fond lisse. Les efforts hydrodynamiques qui s'appliquent sur le cylindre sont notamment plus faibles lorsque celui est proche d'un fond rugueux que d'un fond lisse. De plus les coefficients de traînée statique et oscillante sont largement plus faibles dans le cas rugueux que dans le cas lisse. Les coefficients d'inertie présentent moins de différences significatives entre les différents écartements étudiés.

Summary

Submarine cable behaviour is experimentally studied in the frame of the France Energies Marines project STHYF. In order to evaluate on-bottom stability of cables placed on rocky seabed with high roughness and submitted to combined wave and strong current, hydrodynamic loads are measured on a fixed slender cylinder closely fixed to a horizontal plate, with or without large roughness. A specified set of load cases (forced oscillations, current, forced oscillation + current) is considered to assess the hydrodynamic loads acting on the cylinder placed near a wall for varying gap-to-diameter ratios. The roughness effects on cylinder loads and on the flow are studied in detail. The result show a significant difference between rough and smooth bottom configurations. Indeed, the loads measurements and hydrodynamic coefficients are significantly lower with the presence of a rough plate near the cylinder. Especially for drag and oscillatory drag coefficients, however the inertia coefficient presents less differences between the different studied gaps.

1. Introduction

Flow around a cylinder in unbounded condition has been studied extensively because of its interesting flow features and practical applications [1]. On the contrary, the flow around a cylinder in proximity to a wall has been less studied even if this kind of study has direct application to many engineering problems such as power cables of marine renewable energy systems.
In [2], large-eddy simulations are used to investigate the modifications of the wake dynamics and turbulence characteristics behind a circular cylinder placed near a wall for varying gap-to-diameter ratios. In this study, the shear layer transition, stretching, breakdown and turbulence generation have been studied for a Reynolds number of 1440, in the presence of a smooth wall under steady conditions. Submarine pipelines and power cables at intermediate and shallow waters are subjected to wave and current induced forces. In these conditions, the incident flow separates from the cylinder producing a vortex shedding regime in the near field. The flow separation induces drag and lift hydrodynamic forces which become relevant in comparison with the inertia ones.
An essential step for pipeline and power cable design is the accurate evaluation of these hydrodynamic forces. An experimental work on three types of soil has been carried out by *Zhou and al.* [3] in order to study the seabed responses around a marine pipeline under wave and current conditions, but with no forces measurements on the cylinder. *Aristodemo* [4] proposes a numerical model to determine horizontal and vertical components of the hydrodynamic forces on a slender submarine pipeline lying on the sea bed and exposed to non-linear waves plus a current. The comparison between experimental and numerical hydrodynamic forces shows the accuracy of the new model in evaluating the time variation of peaks and phase shifts of the horizontal and vertical wave and current induced forces. Unfortunately, the seabed roughness effect has not been taken into account in these works (or only for small roughness). It is thus necessary to conduct specific studies in order to study the large seabed roughness effects on the structural loads.
In this study, submarine cable behaviour is experimentaly studied in order to study on-bottom stability of cables placed on rocky seabed with high roughness and submitted to combined wave and strong current (up to 5m/s), as for example in the Alderney Race, France. For that purpose, hydrodynamic loads are measured on a fixed slender cylinder closely fixed to a horizontal plate, with or without large roughness. A specified set of load cases (forced oscillations, current, forced oscillation + current) is considered to assess the hydrodynamic loads acting on the cylinder placed near a wall for varying gap-to-diameter ratios.
The present work is organized as follows: in the second section the experimental set-up is presented; afterwards, the roughness effects on cylinder loads are studied in section 3.

2. Experimental set-up

2.1 Flume tank and assembly

Tests were carried out in the wave and current circulating flume tank of IFREMER located in Boulogne-sur-Mer (France). The incoming flow is assumed to be steady and constant inside the test section of 18 m long $\times$ 4 m wide $\times$ 2 m deep. By means of a grid combined with a honeycomb (that acts as a flow straightener) placed at the inlet of the working section, a low turbulent intensity of $I = 1.5$ % is achieved. In this work, the three instantaneous velocity components are denoted (U,V,W) along the (x,y,z) directions respectively (see figure 1). Using the Reynolds decomposition, each instantaneous velocity component is separated into a mean value and a fluctuation part: $U(X,t) = \overline{U(X)} + u'(X,t)$, where an overbar indicates the time average.
A specific assembly is needed to reproduce submarine cable environment, mainly the boundary layer perceived by the cable due to a rough seabed and the wave influence. Combined waves and current effects act on a bottom cylinder as an oscillatory velocity at the seabed of u_m with a period T, and a background current velocity U. Here, we neglect the vertical motion of the fluid due to the wave. We only take into account in this study the horizontal component of the orbital wave velocity on the seabed. So, $u_m = u_m(x,t)$, imposed by the motion of the assembly by a six degrees of freedom motion generator, able to impose horizontal motion of amplitude

0.4 m at a frequency between 0.1 and 0.4 Hz, with a precision better than one mm.

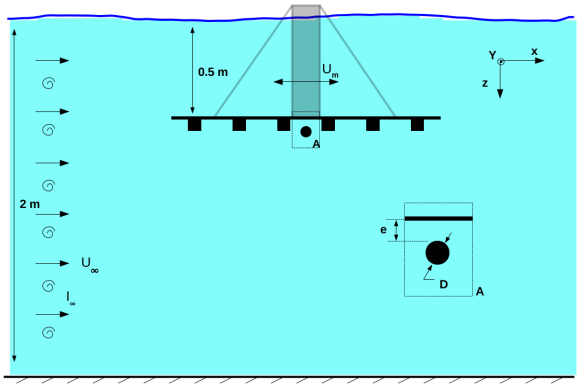

Figure 1. Drawing view of the experimental set-up with the horizontal plate fixed at 0.5 m below the free surface.

The rough seabed is represented by the use of a flat plate (2 m x 1.5 m), fixed horizontally to the motion generator by the use of a specific frame at a depth of 0.5 m from the free surface, as shown in figure 2. Seabed roughness (k_s^{bed}) is here modeled by the use of square blocks fixed on the plate, regularly spaced as shown on figure 1.

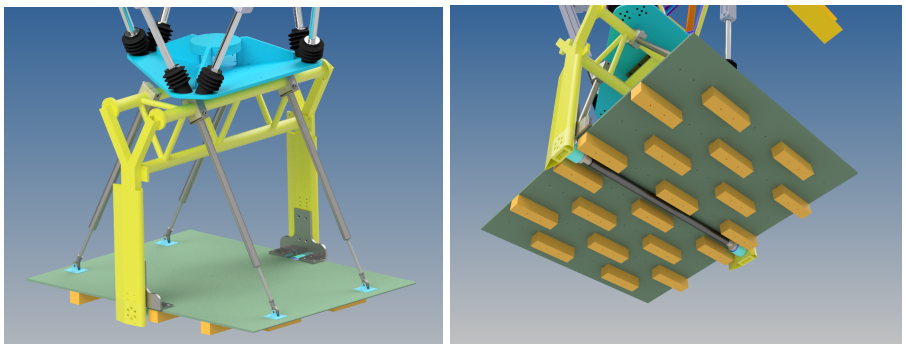

Figure 2. CAD view of the experimental set-up with the frame fixed under the hexapod for the rough bottom configuration.

The cylinder is fixed between two rows of roughness at the center of the plate, perpendicular to the upstream flow. In this study, the model scale is fixed at 1:2.6. Thus, the diameter of the rigid cylinder is fixed at D = 0.05 m and the size of the square blocs at 0.08 m $\times$ 0.08 m $\times$ 0.3 m (see figure 3).

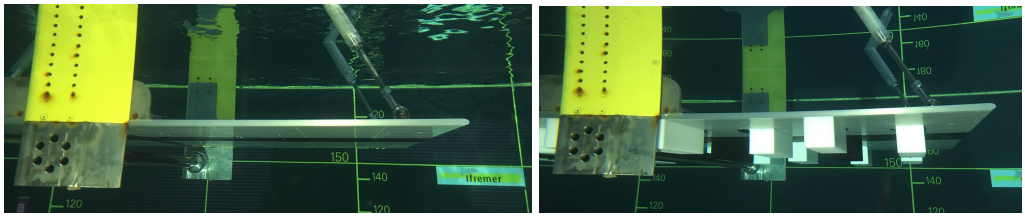

Figure 3. Cylinder fixed under a flat (left) and rough plate (right).

In order to study the boundary layer effects on the cable behaviour, different gaps, denoted e, between the cylinder and the plate have been considered. Four gaps from 2 mm to 2.5 D have been considered with a smooth plate and four gaps from 1 D to 2.5 D with the rough plate, as shown on figure 4. Only one kind of cylinder has been used: a smooth cylinder (weight $\sim 5\ kg$). In the following, non dimensional lengths are used for all parameters indexed by *: $x^* = x/D$, for instance, with D the diameter of the cylinder of length L. The main characteristics of the experimental set-up are summarized in Table 1.

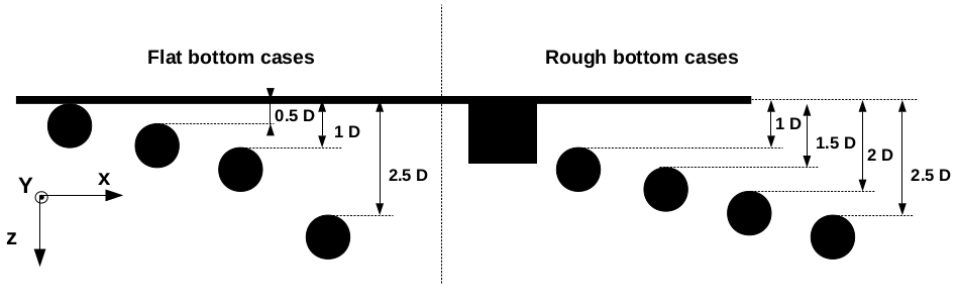

Figure 4. Drawing view of the different configurations, with and without seabed roughness.

Scale -	D $[m]$	e/D -	k_s^{cyl} [m]	k_s^{bed} [m]	U_∞ $[m/s]$
1:1	0.13	[0 ; 2.5]	[0 ; 0.006]	[0.01 ; 0.2]	[0 ; 2.5]
1:2.6	0.05	[0 ; 2.5]	0 - 0.002	0 - 0.08	[0 ; 0.75]

Table 1. *In situ* and experimental conditions.

2.2 Load and flow measurements

Two 2-component force gauges, of range: Fx,z = 100 N, are used to measure the hydrodynamic forces on the cylinder. They are connected at the vertical arm extremity, at each side of the plate, as shown on figure 5. The 1.235 m long cylinder is fixed between them by the mean of needle roller bearings. The cylinder is then free in rotation and translation so as not to exert pre-stress during assembly. No cylinder motions have been encountered during measurements, with comparable measurements between both load-cells (reflecting a perfect forces distribution along the cylinder). The drag and lift forces (respectively F_D and F_L) are then:

$$F_D(t) = F_{x_1}(t) + F_{x_2}(t)$$
$$F_L(t) = F_{z_1}(t) - F_{z_2}(t)$$

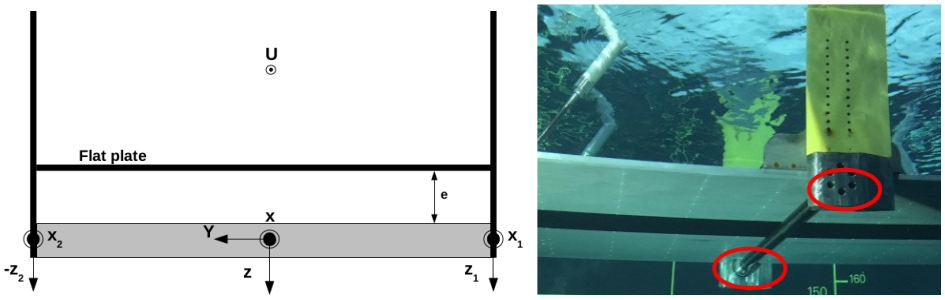

Figure 5. Drawing view of the force measurement system (left) and view of the cylinder fixed between two load cells (surrounded in red) under the smooth plate (right).

The flow around the cylinder location is characterized from PIV (Particle Image Velocimetry) measurements, see figure 6. Beforehand, the tank is seeded with 10 μm diameter silver coated glass particles. A Nd-YAG Laser GEMINI-LIKE is used: power is 200 mJ per probe and wavelength is 532 mm. The laser emission is synchronized with a Camera FLOWSENS EO-2M 1600pix $\times$ 1200pix that makes double images with a time step of 1600 μs.
In these conditions, a particle is detected on 3 to 5 pixels, cross-correlation peak intensity is between 0.3 and 0.8 and peak detectability is 8 in average [5]. PIV acquisitions are made for 150 s, with a 15 Hz acquisition frequency hence 2250 double images are acquired for all cases. The data are post processed with DYNAMIC STUDIO. Particles displacement is calculated using a Cross-Correlation. Outliers are then replaced with the

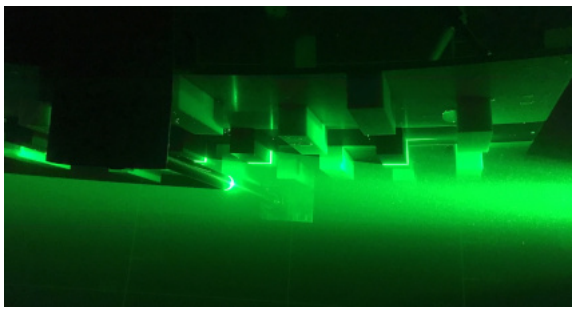

Figure 6. PIV measurement around the smooth cylinder fixed under the rough plate.

Universal Outlier Detection [6], example and precisions on that method can be found in [7]. PIV measurements are carried out in the main axis of symmetry of the assembly, in the plane $y = 0$. The laser illuminates the $y = 0$ plane and the camera is positioned perpendicular to the flow, next to the tank window. PIV uncertainty is estimated to be around 3 %.
The velocity maps obtained for a upstream flow velocity $U = 0.75\ m/s$ are given in figure 7 for the configuration with and without seabed roughness. The results show that the flow under the smooth plate is uniform all over the plate with a boundary layer lower than $1/2\ D$. For the rough case, a large boundary layer of the order of $5D$ is encountered at the cylinder location. This lower velocity will have a significant impact on the results of the calculated coefficients.

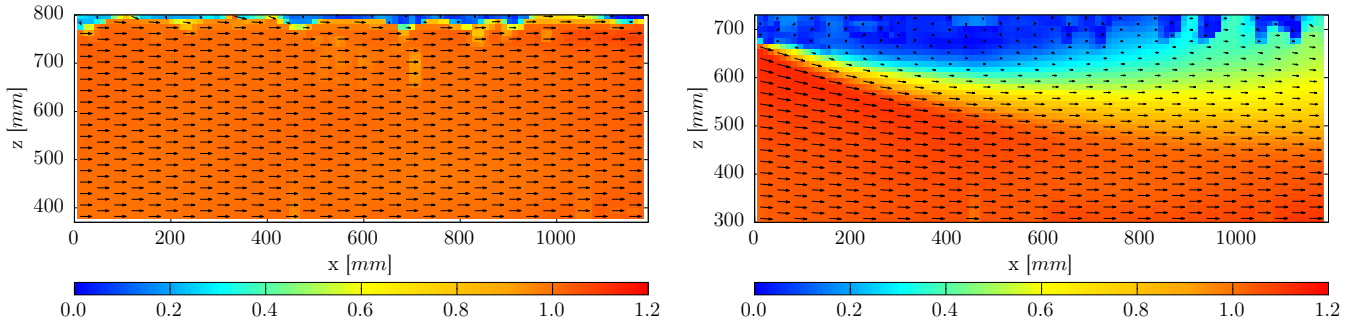

Figure 7. Velocity maps illustrating the boundary layer development under a smooth (left) and rough plate (right).

2.3 Test cases and calculation method of hydrodynamic coefficients

The analysis of hydrodynamic loads acting on a cylinder is usually related to the Keulegan-Carpenter number (KC), the Reynolds number (Re) and the reduced velocity (U_r). They are expressed as:

$$KC = 2\,\pi\,\frac{A_x}{D} \tag{1}$$

$$Re = \frac{UD}{\nu} \tag{2}$$

$$U_r = \frac{UT}{D} \tag{3}$$

The table 2 provides the main geometric characteristics of both studied configurations and summarizes the main test conditions which have been imposed to the tested configurations. A_x and f correspond to the motions amplitude and frequency imposed by the hexapod to simulate the horizontal component due to the waves.
The drag coefficient due to the flow, called *steady-flow drag coefficient*, is calculated as follow:

$$C_D = \frac{2 \times \overline{F_D(t)}}{\rho S U^2} \tag{4}$$

Configuration	D $[m]$	e/D -	k_s^{cyl}/D -	k_s^{bed}/D -	U $[m/s]$	A_x $[mm]$	f $[Hz]$	$Re/10^4$ -	KC -
flat plate	0.05	0 - 2.5	0	0	0.25 - 0.75	100 - 400	0.1 - 0.4	0.125 - 0.375	12 - 50
rough plate	0.05	0 - 2.5	0	1.6	0.25 - 0.75	100 - 400	0.1 - 0.4	0.125 - 0.375	12 - 50

Table 2. Main geometric characteristics and test conditions imposed to the tested configurations

with ρ the density of water ($\rho = 998\ kg/m^3$), $S = D \times L$ the cylinder section in front of the flow and U the current velocity. The notation $\overline{F_D(t)}$ indicates the temporal mean of the drag $F_D(t)$.
In the case of oscillating motions, the hexapod moves along the Ox axis, colinear to the current. The hexapod movements are oscillating with an amplitude A_x and a pulse $\omega = 2\pi f$ such as: $x(t) = A_x \cos(\omega t + \varphi_x)$. It is assumed that the response of this excitation is a sinusoidal function as well (with F_m the amplitude, the harmonics higher than 1 are neglected). Thus, the drag force may be expressed as follows:

$$F_D(t) = F_m \cos(\omega t + \varphi_F) \tag{5}$$

Hence, with $\varphi = \varphi_F - \varphi_x$ it comes :

$$F_D(t) = -\frac{F_m \cos(\varphi)}{A_x\, \omega^2}\, \ddot{x}(t) + \frac{F_m \sin(\varphi)}{A_x\, \omega}\, \dot{x}(t) \tag{6}$$

This equation 6 can be compared with the Morison equation [8] :

$$F_D(t) = -\rho C_m L \frac{\pi D^2}{4}\, \ddot{x}(t) + \frac{1}{2}\rho C_d D L\, \dot{x}(t)\, |\dot{x}(t)| \tag{7}$$

with C_m the inertia coefficient and C_d the drag coefficient. Moreover, $\sin\omega t\ |\sin\omega t|$ can be approximated with $\sin\omega t$, and more precisely with :

$$\sin\omega t\ |\sin\omega t| \simeq \frac{8}{3\pi} \sin\omega t \tag{8}$$

And finally, by comparison :

$$\begin{cases} C_m = \dfrac{F_m \cos(\varphi)}{\rho L \frac{\pi D^2}{4} A_x\, \omega^2} \\ \\ C_d = \dfrac{F_m \sin(\varphi)}{\frac{4}{3\pi}\rho D L A_x^2\, \omega^2} \end{cases} \tag{9}$$

These coefficients are the same as the standard API [9] and are called *Inertia and Drag Coefficients*.
For current and imposed wave-type motion cases it is assumed that the drag force can be divided into two parts, the mean drag part $\overline{F_D(t)}$ and the oscillating part $F_m \cos(\omega t + \varphi_F)$, such as :

$$F_D(t) = \overline{F_D(t)} + F_m \cos(\omega t + \varphi_F) \tag{10}$$

Thus, the three coefficients C_D, C_m ans C_d can be calculated similarly as previous (equations 4 and 9).

3. Roughness effect on cylinder loads

3.1 Current only test

The figure 8 presents the evolution of the mean drag loads as a function of the flow speed for the flat plate configuration (left) and the rough plate configuration (right) for each gap between the cylinder and the plate (see figure 4). In the studied flow range, there is a significant drag force difference between the two configurations. For the flat plate, the drag force reaches approximately 20 N whereas for the rough plate the max of

the drag force reaches 7 N. Moreover, in the flat case there is a difference of about 25% between the smaller gap and the other cases, this difference does not apply in the rough plate configuration where the evolution is more homogeneous. The choice has been made to represent the standard deviation of each measurement represented by the error bars on the graph. The results show that the standard deviation is relatively low in both cases, about 5% of the higher measurement in the flat plate configuration and about 12% for the rough one.

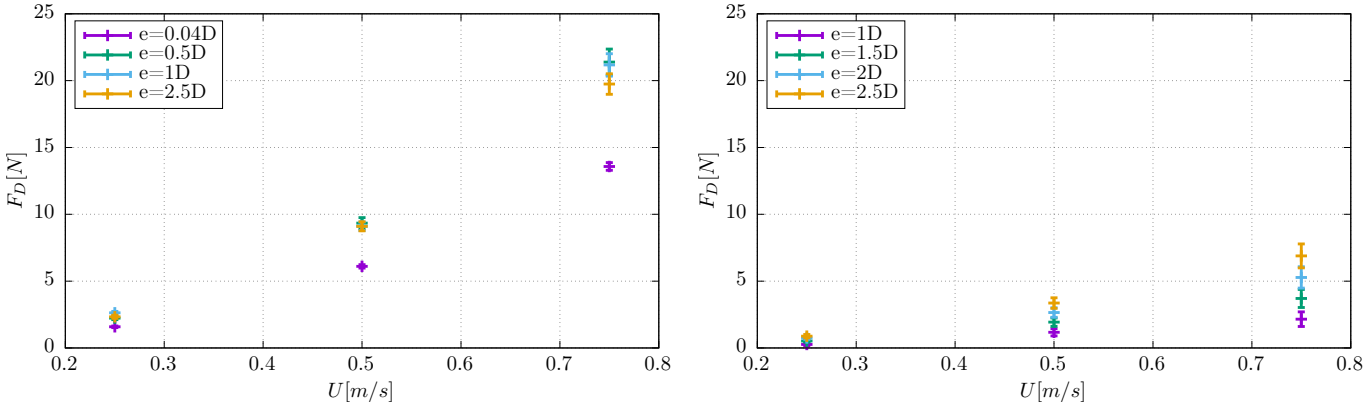

Figure 8. Drag force vs flow speed for the flat plate (left) and the rough one (right).
Error bars represents the standard deviation of the measurement.

These figures highlight that there are no big fluctuations of the drag forces in current only cases even if the fluctuation is slightly higher with the presence of rough bottom. This phenomenom can be explain by the fact that in the studied gap range $(1-2.5D)$, the cylinder stays inside the boundary layer developed by the presence of roughness and equal to approximately $5D$, as we can see in the figure 7 (right), while for the smooth plate, the cylinder is in the boundary layer only for the first gap ($e = 0.004\ D$).

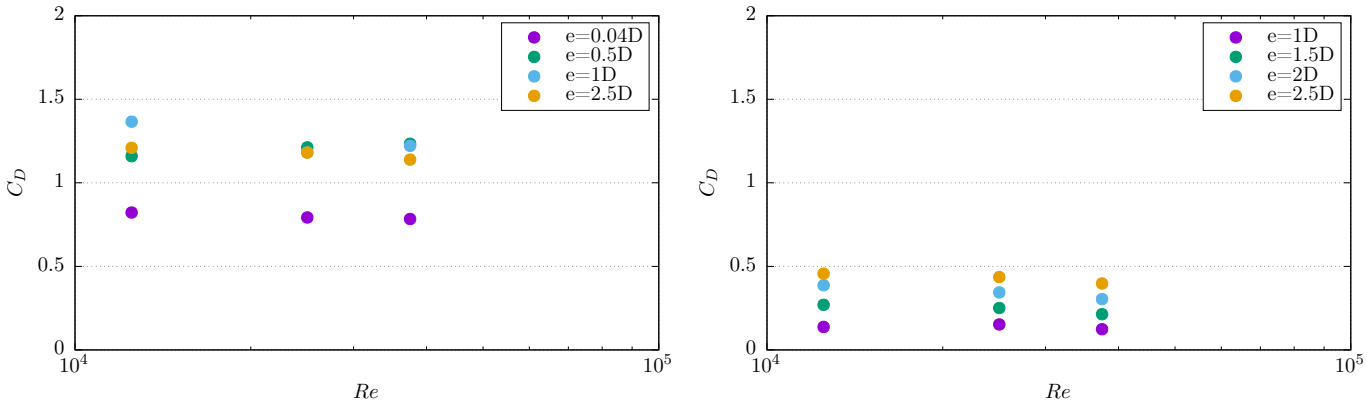

Figure 9. Drag coefficient C_D vs Reynolds number for the flat plate (left) and the rough plate (right).

The variation of the mean drag coefficient C_D for both configurations is presented in the figure 9. The calculated range values is significantly higher for the flat plate case which is between 0.82 for the smaller gap (0.04D) and 1.36 for the bigger one (2.5D). The values of C_D in the flat plate configuration and relatively far from the plate are close to those provided in the research literature for a circular cylinder in a steady flow (see [10]), whereas for the rough configuration the values range is between 0.12 for the smaller gap, and 0.39 for the bigger one. Overall, the closer the plate and the cylinder are, the lower the drag coefficient and the drag forces are. Here the coefficients are calculated from the upstream flow speed (U_∞) and not with the one perceived by the cylinder. In the boundary layer induced by the roughness, the local flow velocity perceived by the cylinder is 5 to 10 times lower than the upstream flow speed. The associated drag coefficient can then reach high values.

Figure 10 presents the dependency of the Strouhal number, $S_t = \frac{f \times D}{U}$, on the Reynolds number. In this formula, f corresponds to the first excitation frequency of the lift force measured on the cylinder. A constant value of $S_t = 0.2$ is observed for the smooth configuration. This value is very close to the Strouhal number commonly used which is generally equal to 0.21, see [11]. For the rough configuration, the Strouhal number drops to a value of about 0.1.

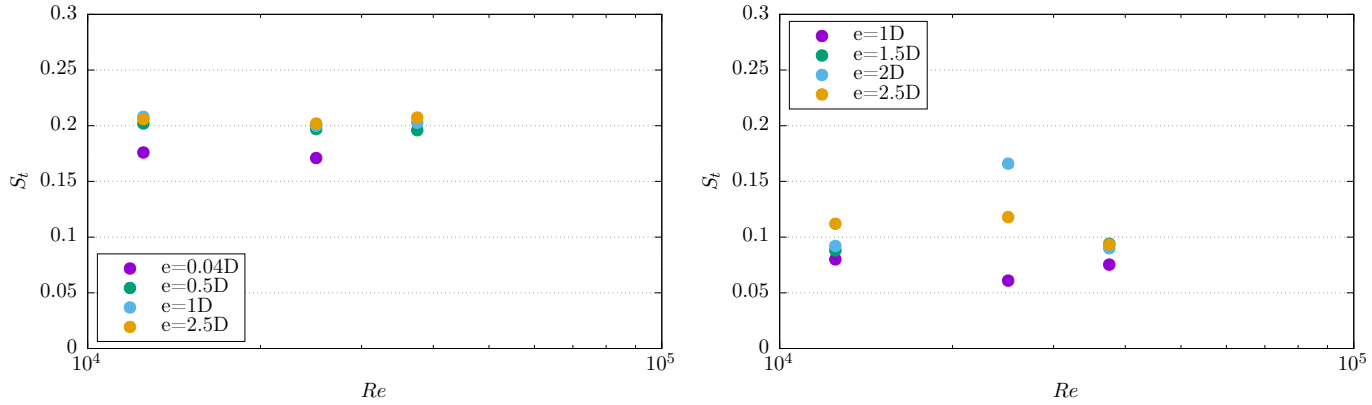

Figure 10. Experimental Strouhal number vs Reynolds number for the flat plate (left) and the rough plate (right).

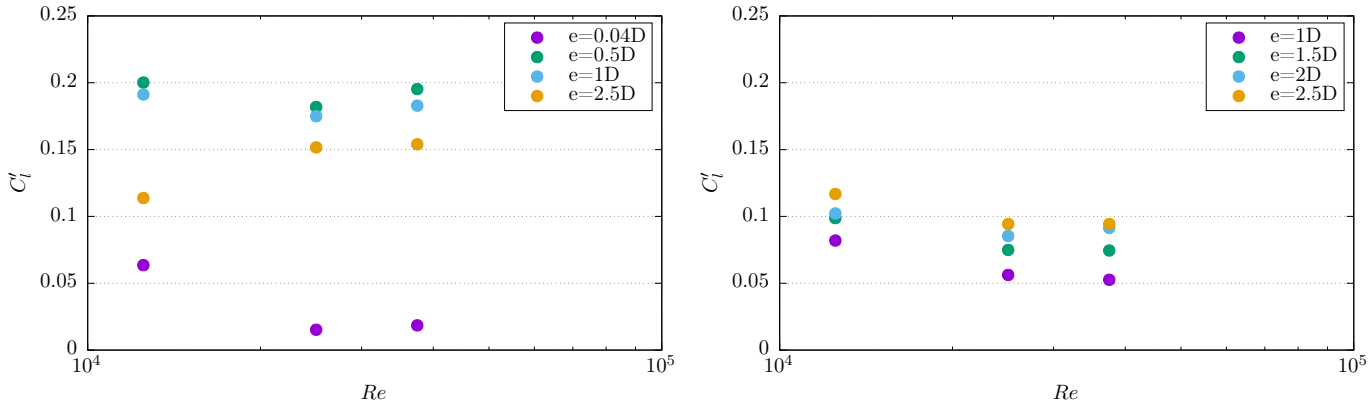

Figure 11. Lift coefficient standard deviation C_l vs Reynolds number for the flat plate (left) and the rough plate (right).

The variation of the r.m.s values of the lift fluctuations with the Reynolds number is shown in figure 11. In the flat plate configuration, a maximum value of approximately 0.2 is obtained for range values of studied Reynolds numbers and for medium gaps ($0.5D$ and $1D$). This value drops to almost zero in the closer gap case. In the rough plate configuration, the variation of C_l' is more homogeneous and shows a slight decrease for each gap, between 0.05 and 0.1.
These results show that the rough bottom has an influence on the drag coefficient, the r.m.s. values of the lift fluctuations and the Strouhal number. The vortices are shed into the wake with different frequencies.

3.2 Oscillating motions

The figure 12 presents the evolution of the mean drag forces in function of K_c for the flat plate case (left) and the rough plate case (right) for the oscillating motion test cases. The standard deviation of each measurement is represented by the error bars on the graph. There are several points at each K_c studied because several tests have been carried out at the same motion amplitude A_x but with different frequencies. As expected the mean drag loads is equal to zero for both configurations as there is no current, but the standard deviation calculated for each test shows that it increases for the smooth plate case, by a factor of two approximately.

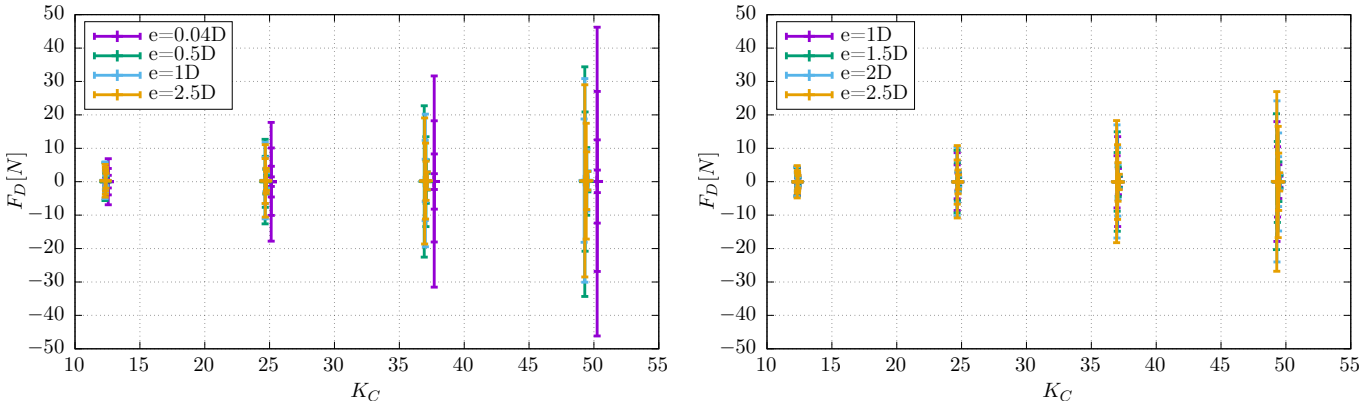

Figure 12. Drag force vs Reynolds number for the flat plate on the left and the rough plate on the right. *Error bars* represents the standard deviation of the measurement.

The evolution of the oscillating drag coefficient C_d for the flat plate case (left) and the rough plate case (right) in function of K_c is represented in the figure 13. The calculated range values of the flat plate case is between 1.2 for the smaller gap (0.04D) and 2.6 for the bigger gap (2.5D). For the rough configuration the range values is between 0.25 for the 1D gap and 2 for the 2.5D gap. This comparison does not highlight significant differences for the maximum range values. However, for the rough configuration the minimum value is decreased by a factor of 4 compared to the flat plate configuration.

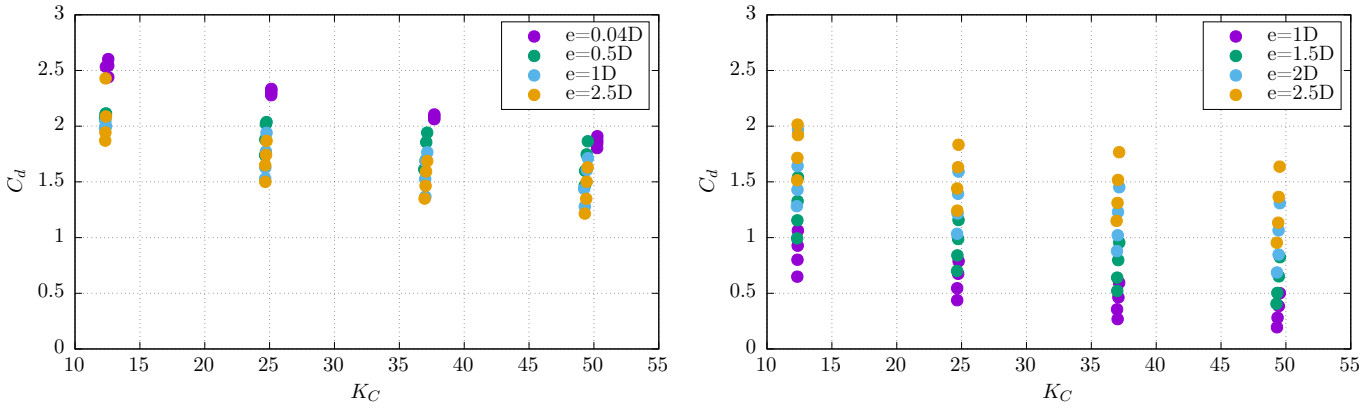

Figure 13. Oscillating drag coefficient C_D vs K_C for the flat plate on the left and the rough plate on the right.

The figure 14 shows similarly the inertia coefficient C_m as a function of K_C. The calculated range values is between 0.8 and 6 for the flat configuration and between 1 and 3 for the rough one. The presence of a rough plate in vicinity of the cylinder reduces significantly the inertia coefficient. In both cases, calculated coefficients show an opposite behaviour concerning the gap between the cylinder and the plate. We clearly see that the higher values are for the smaller gap case in the flat plate configuration. Whereas in the rough plate configuration, the closer case ($1D$) has the lower values. Overall, the behaviour of the cylinder shows that oscillating drag coefficients and inertia coefficients are significantly lower with the presence of a rough plate.

3.3 Current and oscillating motions

The present section outlines results concerning current and oscillating motions tested cases. The figure 15 shows the evolution of the mean drag force in function of the reduced speed U_r for the flat plate case (left) and the rough plate case (right) for each gap between the cylinder and the plate. As previously, the standard deviation of each measurement is represented by an error bar on the graph.
Contrary to the oscillating motion only case, the mean drag forces are not equal to zero anymore, especially

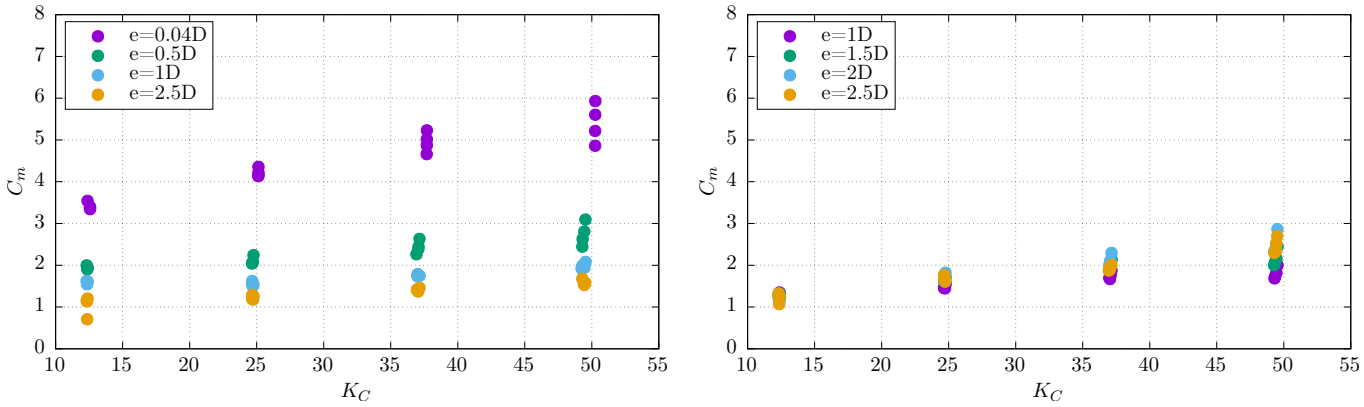

Figure 14. Added mass coefficient C_m vs K_C for the flat plate on the left and the rough plate on the right.

in the flat plate case where the mean drag force can reach 39 N for a K_c equal to 38. However, in the rough plate configuration, these mean drag forces reach a maximum of 10 N for a K_c equal to 38 but is less than 5 N in most cases with a small standard deviation as if it was in an oscillating motion only configuration. The presence of the rough plate near the cylinder reduces both mean drag forces and standard deviation by 30%.

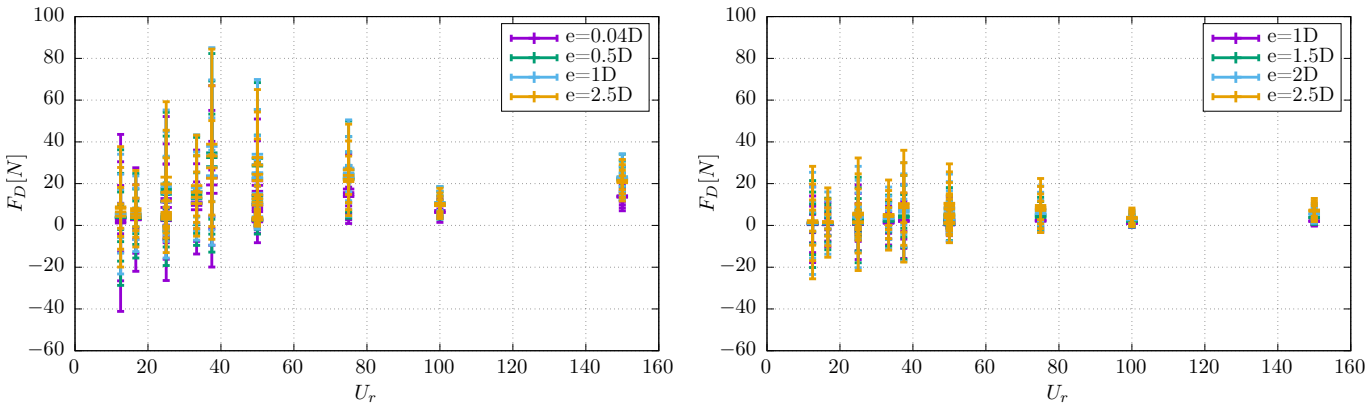

Figure 15. Drag force vs Reduced velocity U_r for the flat plate on the left and the rough plate on the right. *Error bars* represents the standard deviation of the measurement.

The same coefficients previously shown, the mean drag coefficient C_D, the oscillating drag coefficient C_d and the added mass coefficient C_m are respectively represented in the figures 16, 17 and 18 in function of the reduced speed U_r .

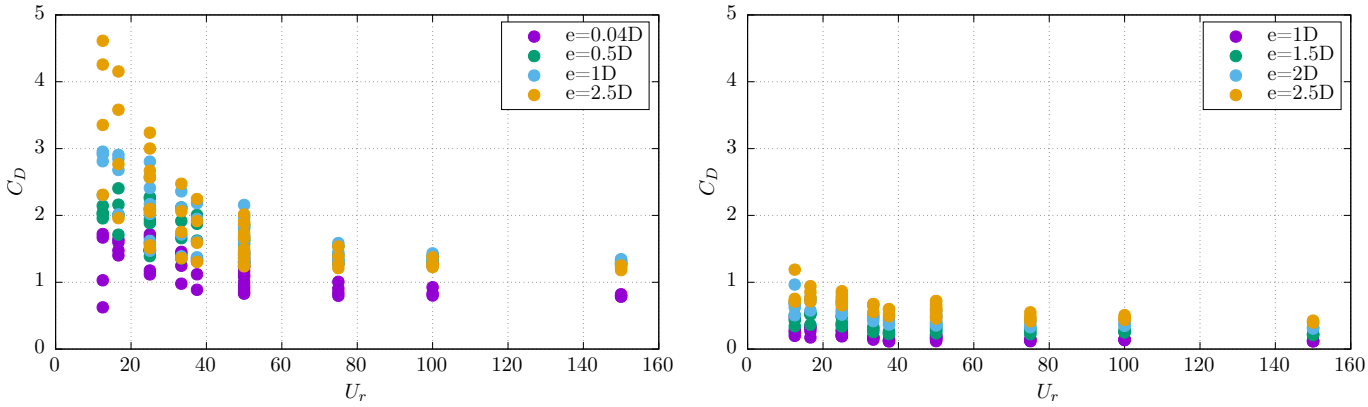

Figure 16. Mean drag coefficient C_D vs Reduced velocity U_r for the flat plate on the left and the rough plate on the right.

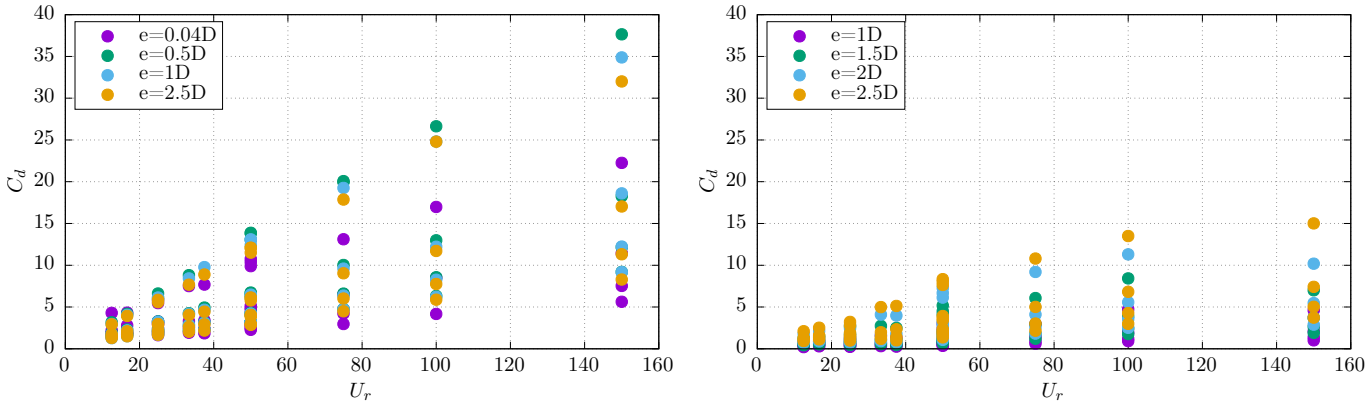

Figure 17. Oscillating drag coefficient C_d vs Reduced velocity U_r for the flat plate on the left and the rough plate (right).

The mean drag coefficient C_D and the oscillating drag coefficient C_d are significantly higher in the case of the flat plate configuration compare to the rough one. Almost four times higher for C_D and more than two times higher for C_d. As seen previously, the roughness drastically decreases the parameter values linked to drag phenomena by decreasing locally the mean flow speed. A change of behaviour is clear at $U_r \approx 60$. For $U_r \leq 60$, the cylinder behaviour is mainly driven by the static drag for both kinds of bottom while for $U_r \geq 60$ the cylinder behaviour is driven by the oscillating drag and the inertia coefficient (whatever the gap is).

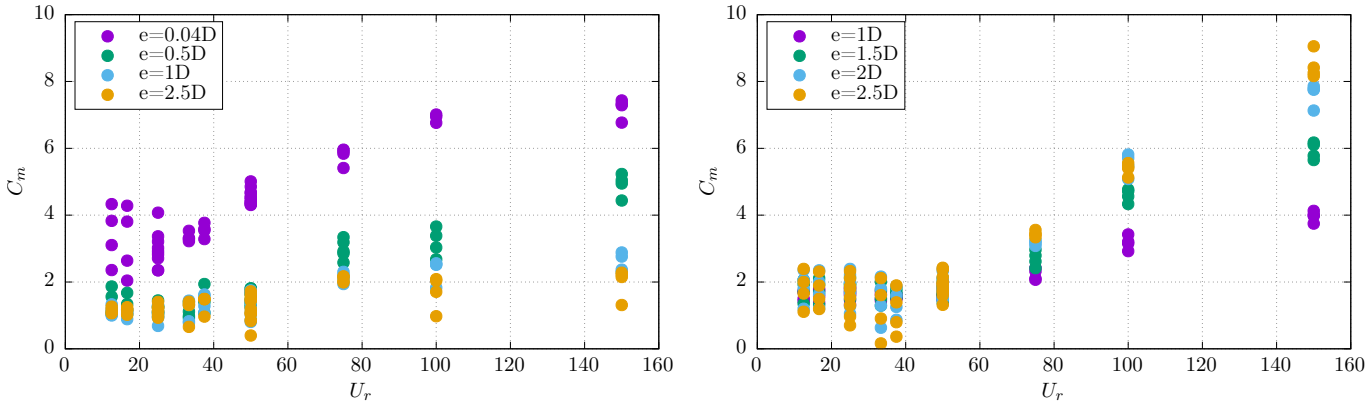

Figure 18. Added mass coefficient C_m vs Reduced velocity U_r for the flat plate on the left and the rough plate (right).

Moreover the roughness seems to have less impact on inertia phenomena. Indeed, the range values of the added mass is nearly the same in presence of a smooth or a rough bottom as we can see in figure 18.
Furthermore, as for the oscillating case, the behavior of the C_m coefficient is opposite if we are in rough or flat configuration. We clearly see that the higher values are for the case $0.04D$ in the flat plate configuration, whereas in the rough plate configuration, the closer case ($1D$) has the lower values.

4. Conclusion and Perspectives

This study shows the impact of a plate with large roughness on the drag and inertia coefficients measured on a cylinder located near to it. The results are compared to the results obtained with a smooth bottom configuration. From these results, the evolution of the drag and inertia coefficients measured on the cylinder submitted to several test conditions (forced oscillations, current, forced oscillation + current) can be studied. Results show that a rough bottom has an important impact on the hydrodynamic forces acting on a cylinder, especially for mean and oscillating drag coefficient. The drag forces due to a constant flow are more than 50% lower in the rough configuration, and it can be explain by the PIV study which shows how much the flow field can be

perturbated by the presence of the roughness. Indeed, the presence of a rough plate generates a large boundary layer where the velocity flow drops drastically. Overall, the closer the plate and the cylinder are, the lower the drag coefficient and the drag forces are. Here the coefficients are calculated from the upstream flow speed (U_∞) and not with the one perceived by the cylinder. In the boundary layer induced by the roughness, the local flow velocity perceived by the cylinder is 5 to 10 times lower than the upstream flow speed. The associated drag coefficient can then reach high values. The same trends for the oscillating motions and oscillating motions with current can be made concerning drag coefficients. For added mass coefficients, the study does not highlight significant differences between the flat plate configuration and the rough one.
Moreover these results show that the rough bottom has an influence on the the r.m.s. values of the lift fluctuations and the Strouhal number. The vortices are shed into the wake with different frequencies. The r.m.s. values of the drag forces are generally lower for the rough configuration by about 30%, except in current only where there are no significant differences.

Acknowledgment

This work benefited from France Energies Marines and State financing managed by the National Research Agency under the Investments for the Future program bearing the reference ANR- 10-IED-0006-20. This project was partly financially supported by the European Union (FEDER), the French government, IFREMER and the region Hauts-de-France in the framework of the project CPER 2015-2020 MARCO.

References

[1] C. Willimason, "Vortex dynamics in the cylinder wake," *Annual Review of Fluid Mechanics*, vol. 28, pp. 477–539, 1996.

[2] S. Sarkar and S. Sarkar, "Vortex dynamics of a cylinder wake in proximity to a wall," *Journal of Fluids and Structures*, vol. 26, pp. 19–40, 2010.

[3] C. Zhou, G. Li, P. Dong, J. Shi, and J. XU, "An experimental study of seabed responses around a marine pipeline under wave and current conditions," *Ocean Engineering*, vol. 38, pp. 226–234, 2011.

[4] F. Aristodemo, G. Tomasiccho, and P. Veltri, "New model to determine forces at on-bottom slender pipelines," *Coastal Engineering*, vol. 58, pp. 267–280, 2011.

[5] R. Adrian and J. Westerweel, "Particle image velocimetry," *Cambridge Univ. Press, Cambridge*, 2011.

[6] J. Westerweel and F. Scarano, "Universal outlier detection for PIV data," *Exp. Fluids*, vol. 39, 2005.

[7] M. Ikhennicheu, G. Germain, P. Druault, and B. Gaurier, "Experimental study of coherent flow structures past a wall-mounted square cylinder," *In Press in Ocean Engineering*, 2019.

[8] J. R. Morison, M. P. O'Brien, J. W. Johnson, and S. A. Schaaf, "The forces exerted by surface waves on piles," *Journal of Petroleum Technology*, vol. 2, pp. 149–154, May 1950.

[9] American Petroleum Institute (API), "Planning, Designing and Constructing Fixed Offshore Platforms - Working Stress Design," *API Recommended Practice 2A-WSD (RP 2A-WSD)*, 2000.

[10] G. Schewe, "On the force fluctuations acting on a circular cylinder in crossflow from subcritical up to transcritical reynolds numbers," *J. Fluid Mechanics*, vol. 133, pp. 265–285, 1983.

[11] W. H. Melbourne and H. M. Blackburn, "The effect of free-stream turbulence on sectional lift forces on a circular cylinder.," *J. Fluid. Mech.*, vol. 11, pp. 267–292, 1996.